BIOCHEMISTRY
including biophysical chemistry & molecular biology

Article

pubs.acs.org/biochemistry

Pre-Steady-State Kinetic Analysis of 1-Deoxy-D-xylulose-5-phosphate Reductoisomerase from *Mycobacterium tuberculosis* Reveals Partially Rate-Limiting Product Release by Parallel Pathways

Juan Liu[†] and Andrew S. Murkin*

Department of Chemistry, University at Buffalo, The State University of New York, Buffalo, New York 14260, United States

Supporting Information

ABSTRACT: As part of the non-mevalonate pathway for the biosynthesis of the isoprenoid precursor isopentenyl pyrophosphate, 1-deoxy-D-xylulose-5-phosphate (DXP) reductoisomerase (DXR) catalyzes the conversion of DXP into 2-*C*-methyl-D-erythritol 4-phosphate (MEP) by consecutive isomerization and NADPH-dependent reduction reactions. Because this pathway is essential to many infectious organisms but is absent in humans, DXR is a target for drug discovery. In an attempt to characterize its kinetic mechanism and identify rate-limiting steps, we present the first complete transient kinetic investigation of DXR. Stopped-flow fluorescence measurements with *Mycobacterium tuberculosis* DXR (*Mt*DXR) revealed that NADPH and MEP bind to the free enzyme and that the two bind together to generate a nonproductive ternary complex. Unlike the *Escherichia coli* orthologue, *Mt*DXR exhibited a burst in the oxidation of NADPH during pre-steady-state reactions, indicating a partially rate-limiting step follows chemistry. By monitoring NADPH fluorescence during these experiments, the transient generation of *Mt*DXR·NADPH·MEP was observed. Global kinetic analysis supports a model involving random substrate binding and ordered release of $NADP^+$ followed by MEP. The partially rate-limiting release of MEP occurs via two pathways—directly from the binary complex and indirectly via the *Mt*DXR·NADPH·MEP complex—the partitioning being dependent on NADPH concentration. Previous mechanistic studies, including kinetic isotope effects and product inhibition, are discussed in light of this kinetic mechanism.

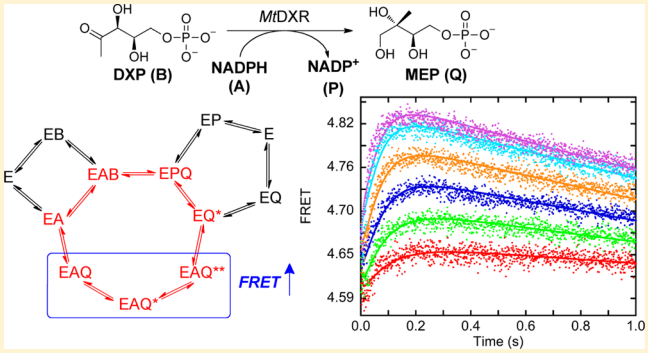

The mevalonate pathway is present in eukaryotes for isoprenoid synthesis. In contrast, many bacteria including pathogens such as *Mycobacterium tuberculosis* synthesize isoprenoids via the non-mevalonate pathway.[2,3] This pathway begins with the thiamine diphosphate-dependent synthesis of 1-deoxy-D-xylulose-5-phosphate (DXP) catalyzed by DXP synthase via a condensation reaction from pyruvate and glyceraldehyde 3-phosphate accompanied by decarboxylation.[4] DXP in turn is converted into 2-*C*-methyl-D-erithritol 4-phosphate (MEP), which ultimately leads to the end-products isopentenyl pyrophosphate and dimethylallyl pyrophosphate. The generation of MEP from DXP is accomplished by consecutive rearrangement and NADPH-dependent reduction steps within the active site of DXP reductoisomerase (DXR). DXR, like all enzymes of the non-mevalonate pathway, is a potential target for antimicrobial drugs, and knowledge of its chemical and kinetic mechanism is indispensable for inhibitor design.

During the DXR-catalyzed reaction, DXP undergoes a ketose−aldose isomerization,[5] likely via a retroaldol/aldol mechanism,[6] followed by reduction to the alditol MEP. Although the isomerization−reduction is reversible, the overall process favors the reduction direction. A divalent metal ion is required as an activator for catalysis. Whereas Co^{2+} and Mn^{2+} have been shown to have lower K_{act} values for *Mt*DXR, Mg^{2+} may likely serve as the physiologically relevant activator.[7]

Despite the extensive studies performed on DXR under steady-state conditions, several mechanistic uncertainties remain. Steady-state kinetics and kinetic isotope effects (KIEs) reported by Argyrou and Blanchard suggest a steady-state random mechanism for *Mt*DXR.[7] Product inhibition studies, however, intriguingly revealed a single competitive pattern—that of MEP against DXP—a result that is consistent with an ordered mechanism with DXP and MEP binding to free enzyme. In contrast, studies on *E. coli* DXR suggested an ordered mechanism with NADPH binding first.[8] Further, hydride transfer and a product release step or conformational change were suggested as partially rate-limiting steps.[7] The identity of these steps remains to be determined.

Through the use of steady-state and transient kinetics, we present a complete kinetic model for *Mt*DXR and address several mechanistic uncertainties. We evaluate the preferred

Received: April 19, 2012
Revised: June 4, 2012
Published: June 12, 2012

   dx.doi.org/10.1021/bi300513r | *Biochemistry* 2012, 51, 5307−5319

order of substrate binding and product release and identify the rate-limiting step in turnover. Contrary to previous models, our results implicate MEP rather than $NADP^+$ as the second product to be released. Observation of a nonproductive ternary complex with NADPH and MEP revealed that partially rate-limiting release of MEP occurs via two parallel pathways.

EXPERIMENTAL PROCEDURES

Materials. All chemicals were of analytical or reagent grade and were used without further purification unless otherwise stated. D-[1-^{3}H(N)]Glucose (20 Ci/mmol) was purchased from Moravek. Chicken muscle triosephosphate isomerase[9] and *E. coli* DXP synthase[7] were expressed and purified as reported using their corresponding plasmids obtained as gifts from Profs. John P. Richard (University at Buffalo) and John S. Blanchard (Albert Einstein College of Medicine), respectively. Rabbit muscle aldolase was obtained from commercial sources. The gene encoding *Mt*DXR was obtained synthetically (DNA 2.0, Menlo Park, CA) inserted into the pJexpress 404 vector by the supplier. The DNA sequence was optimized for *E. coli* codon usage and encodes a thrombin-cleavable N-terminal His_6-tag (MHHHHHHLVPRGSH) fused to the first 389 residues[10] of the native protein from *M. tuberculosis* strain H37R.[11]

Expression and Purification of *Mt*DXR. BL21(DE3) *E. coli* cells transformed by the supplier (DNA 2.0) with the plasmid encoding *Mt*DXR were grown at 37 °C to an OD_{600} of 0.5−0.6 in 10 L of LB-Miller broth containing 100 mg/L ampicillin. The cells were cooled to 31 °C, and protein expression was induced with 0.5 mM IPTG for 4−5 h. Cells were harvested by centrifugation and resuspended in Buffer A (50 mM Tris, 0.5 M NaCl, 30 mM imidazole, 10% glycerol, adjusted to pH 7.5 at 25 °C with HCl), supplemented with a protease inhibitor cocktail and 5−10 mg of DNase I. Cells were lysed by high-shear disruption using a Microfluidizer M-110L (Microfluidics), and the lysate was clarified by centrifugation at 15000*g* for 30 min at 4 °C. The supernatant was loaded onto a HisPrep FF16/10 column (GE Healthcare; column volume, CV = 20 mL) containing Ni·NTA resin, equilibrated with Buffer A. The column was washed with 100 mL (5 CV) of Buffer A and eluted with a linear 0−60% gradient (300 mL; 15 CV) against Buffer B (Buffer A plus 0.5 M imidazole) using an ÄKTA Explorer 10 FPLC system (GE Healthcare). Fractions were analyzed by SDS-PAGE, pooled, and concentrated with an Amicon ultrafiltration device (10 kDa MWCO membrane). The concentrated protein was dialyzed against dialysis buffer (50 mM Tris, 100 mM NaCl, 5 mM $MgCl_2$, and 10% glycerol, adjusted to pH 7.5 at 25 °C with HCl), flash frozen in liquid nitrogen, and stored at −80 °C. Protein concentrations were determined spectrophotometrically using the extinction coefficient (ε_{280} = 37 500 M^{-1} cm^{-1}) calculated from its amino acid sequence using the ProtParam utility[12] and verified by Bradford assay.

Synthesis of DXP and MEP. DXP was synthesized enzymatically by *E. coli* DXS from pyruvate and D-glyceraldehyde 3-phosphate, which was generated by the action of aldolase and TIM from fructose 1,6-bisphosphate.[7,13] MEP was synthesized enzymatically from DXP using *Mt*DXR and a NADPH-regeneration system.[14] Following ultrafiltration to remove proteins and concentration by rotary evaporation, DXP and MEP were dissolved in THF/H_2O (2:1, v/v) and purified by chromatography on cellulose.[6] Fractions were identified by *p*-anisaldehyde staining, pooled, and concentrated by rotary evaporation. To remove residual UV-absorbing contaminants, the residue was dissolved in water and passed through a 5 mL column of activated charcoal, previously rinsed with 10% ethanol. The pooled DXP and MEP fractions were concentrated and stored at −20 °C.

Steady-State Kinetics and Product Inhibition. NADPH and $NADP^+$ concentrations were determined spectrophotometrically at 340 nm (ε_{340} = 6.22 mM^{-1} cm^{-1}) and 260 nm (ε_{260} = 17.8 mM^{-1} cm^{-1}), respectively.[15] DXP and MEP concentrations were determined by ^{1}H NMR (120 s delay between transients) with 5 mM imidazole as an internal standard.[16] Initial velocities were measured spectrophotometrically at 340 nm (ε_{340} = 6.22 mM^{-1} cm^{-1}). For each reaction direction, one substrate was varied with the cosubstrate fixed at a saturating concentration. Specifically, the following concentrations were used: NADPH (2−400 μM) with 2 mM DXP, DXP (25−4000 μM) with 200 μM NADPH, $NADP^+$ (20−2000 μM) with 1 mM MEP, and MEP (20−1500 μM) with 1.6 mM $NADP^+$. Reactions were performed at 25 °C in 50 mM Tris·HCl, pH 7.5, containing 10 mM $MgCl_2$, and were initiated by the addition of 20−200 nM *Mt*DXR. Data were fitted with eq 1 to determine $k_{cat,app}$ (left form), $(k_{cat}/K_a)_{app}$ (right form), and K_a:

$$\nu_0 = \frac{k_{cat,app}[E]_0[A]}{K_a + [A]} = \frac{(k_{cat}/K_a)_{app}[E]_0[A]}{1 + [A]/K_a} \quad (1)$$

where $k_{cat,app}$ and $(k_{cat}/K_a)_{app}$ were corrected for the fraction of saturation by the fixed substrate, $[B]/(K_b + [B])$, to obtain the true k_{cat} and k_{cat}/K_a. Product inhibition studies were performed at a fixed concentration of one substrate (either near its K_m or saturating) and variable concentrations of the other substrate at several fixed concentrations of the inhibitor ($NADP^+$).

Transient Kinetics. Transient kinetic studies were performed using an Applied Photophysics SX-20 stopped-flow spectrometer fit with a 20 μL flow cell with a dead time of 1.08 ms. Transients from four to six repeat drives were averaged for all stopped-flow assays. For fluorescence measurements, a 2 mm incident light path length was used to minimize inner filtering effects, and the slit width was set to 2 mm in the excitation monochromator. For absorbance measurements, either a 2 or 10 mm path length was chosen, as indicated. The reaction chamber and all reagents were thermostatted at 25.0 °C with a circulating water bath. All concentrations are given as final after 1:1 mixing, and all solutions contained 50 mM Tris·HCl, pH 7.5 and 10 mM $MgCl_2$.

Data Analysis. After correction for the dead time, data were analyzed by analytical nonlinear regression using Pro-Data Viewer (Applied Photophysics) and KaleidaGraph (Synergy Corp.), and standard errors associated with fitting are reported. Global data simulation was performed using KinTek Global Kinetic Explorer version 3.0 (KinTek Corp.),[17,18] and errors are reported from nonlinear regression and FitSpace confidence contour analysis using a χ^2 threshold of 1.2.[19]

Binding and single-turnover transients were fitted with either single- or double-exponential functions of the form

$$I_t = \sum_i A_i e^{-k_{obs,i}t} + I_{eq} \quad (2)$$

where I_t is the signal intensity at time t, A_i is the amplitude of the ith signal change, $k_{obs,i}$ is an apparent first-order rate constant for the ith transient phase, and I_{eq} is the signal intensity at equilibrium. Goodness of fit was evaluated by examination of the residuals.

dx.doi.org/10.1021/bi300513r | *Biochemistry* 2012, 51, 5307−5319

For single-exponential binding, k_{obs} was fitted with a linear (eq 3) or hyperbolic (eq 4) function, representative of one-step or two-step binding models, respectively

$$k_{obs} = k_1[S] + k_{-1} \quad (3)$$

$$k_{obs} = \frac{k_2[S]}{K_{-1} + [S]} + k_{-2} \quad (4)$$

where k_1, k_{-1}, and K_{-1} are the forward and reverse rate constants and initial dissociation constant and k_2 and k_{-2} are the forward and reverse rate constants governing the slow equilibrium converting the initial, loose encounter complex to a tighter complex. Strictly, eq 4 only holds when $k_{-1} \gg k_2$, which is generally indicated when only one exponential phase is observed over all [S].[20] For double-exponential binding, the observed rate constants for fast (k_{obs1}) and slow (k_{obs2}) phases were fitted with eq 5 and eq 6, respectively

$$k_{obs1} = k_1[S] + k_{-1} + k_2 + k_{-2} \quad (5)$$

$$k_{obs2} = \frac{k_1[S](k_2 + k_{-2}) + k_{-1}k_{-2}}{k_{-1}[S] + k_{-1} + k_2 + k_{-2}} \quad (6)$$

where k_1 is the slope of k_{obs1} versus [S], the sum $k_2 + k_{-2}$ is the maximal rate of k_{obs2} versus [S], and k_{-1} is the difference between the intercept of the former and the maximal rate of the latter. The net dissociation constant, $K_{d,net}$, for the two-step binding, E + S ⇌ ES ⇌ ES*, is defined by eq 7

$$K_{d,net} = \frac{[E][S]}{[ES] + [ES^*]} = \frac{K_{-1}}{1 + K_2} \quad (7)$$

and reflects substrate dissociation from the two complexes at equilibrium. This $K_{d,net}$ was obtained from the substrate dependence of k_{obs2} and the amplitude of the slow phase. Solving for K_2 in eq 7, together with the maximal rate in eq 6, provides solutions for k_2 and k_{-2}.[20]

For pre-steady-state experiments, the region of the transients including the burst and linear steady-state region were fitted with

$$A_t = (\Delta A)e^{-k_{burst}t} + \nu_{ss}t + c \quad (8)$$

where ΔA is the amplitude of the burst, k_{burst} is the apparent first-order rate constant, and ν_{ss} is the steady-state rate, governed by the Michaelis–Menten equation, following the burst. The plot of k_{burst} versus substrate concentration was hyperbolic with no y-intercept, and therefore it was fitted with eq 9[21,22]

$$k_{burst} = \frac{(k_{chem} + k_{off})[B]}{K_d + [B]} \quad (9)$$

where k_{chem} is the net rate constant for conversion of the reactant ternary complex to the product complex immediately preceding the slow step, k_{off} is the net rate constant for the slow product release step, and K_d is the apparent dissociation constant for the second substrate, B, from the ternary complex.[a]

Kinetics of NADPH and MEP Binding to *Mt*DXR. NADPH binding to *Mt*DXR was monitored by the increase of fluorescence resonance energy transfer (FRET) from tryptophan residues to the bound cofactor. The excitation monochromator was set at 290 nm, and emission above 395 nm was detected using a long-pass cutoff filter (Schott). The binding of MEP was monitored by the quench in protein intrinsic fluorescence emission with a 320 nm long-pass filter (Schott). Binding of NADPH (10–140 μM) or MEP (20–2000 μM) to *Mt*DXR (1 μM) was recorded at a rate of 10 points/ms for each transient. In each case, a single-exponential function was best fitted to the transients, and the amplitudes (A) were used to determine dissociation constants using eq 10.

$$A = A_{max}\frac{[S]}{K_d + [S]} \quad (10)$$

Inner filter effects by NADPH were examined by monitoring the fluorescence over the same concentration range in the absence of protein with excitation at 290 and 340 nm. In both cases, a linear plot of fluorescence intensity versus NADPH concentration was obtained, indicating negligible inner filtering under these conditions.

Formation of the nonproductive E·NADPH·MEP complex was monitored by changes in FRET, as described for NADPH binding to the free enzyme. Premixed *Mt*DXR (2 μM) and MEP (1 mM) were mixed with varying concentrations of NADPH (10–140 μM). Alternatively, premixed *Mt*DXR (4 μM) and NADPH (200 μM) were mixed with varying concentrations of MEP (15–1000 μM).

Kinetics of Pre-Steady-State Reactions. To study burst kinetics under multiple turnover conditions in the reduction direction, premixed *Mt*DXR (30 μM) and NADPH (400 μM) were mixed with varying concentrations of DXP (0.2–8 mM) from the second syringe. Absorbance and fluorescence (395 nm cutoff) were monitored simultaneously by excitation at 340 nm (2 mm path length). Alternatively, premixed *Mt*DXR (20 μM) and DXP (2.5 mM) were mixed with varying concentrations of NADPH (40–200 μM) from the second syringe, with monitoring via the absorbance channel (10 mm path length). A split time scale was used with 500 points collected for 0–0.1 s and 5000 points collected for 0.1–5.1 s.

Formation and breakdown of the fluorescent E·NADPH··MEP complex during turnover conditions were monitored by changes in FRET (290 nm excitation) as described earlier for binding experiments. *Mt*DXR (1 μM) was premixed with saturating concentrations of either NADPH (200 μM) or DXP (1 mM) and mixed with varying concentrations of the second substrate.

To study pre-steady-state kinetics under multiple turnover conditions in the oxidation direction, premixed *Mt*DXR (20 μM) and MEP (500 μM) were mixed with varying concentrations of $NADP^+$ (0.2–2 mM) from the second syringe. Alternatively, premixed *Mt*DXR (20 μM) and $NADP^+$ (1.5 mM) were mixed with varying concentrations of MEP (50–500 μM) from the second syringe. In both cases, absorbance at 340 nm (10 mm path length) was monitored with a split time scale of 2000 points for 0–0.25 s and 500 points for 0.25–2.25 s.

RESULTS AND DISCUSSION

Steady-State Kinetics. The recombinant *Mt*DXR studied previously was notably unstable and required several purification steps.[7] We chose to express an N-terminal His_6-fusion of the first 389 of 413 residues, as this construct has been reported to be stable with similar kinetic properties.[10] Steady-state kinetic studies for the forward (reduction) and reverse (oxidation) reaction directions were performed in the presence of saturating Mg^{2+} (10 mM) with one substrate varied at a

dx.doi.org/10.1021/bi300513r | *Biochemistry* 2012, 51, 5307–5319

Table 1. Steady-State Kinetic Parameters for *Mt*DXR[a]

substrate		kinetic parameter		
		k_{cat} (s^{-1})	K_m (μM)	k_{cat}/K_m (M^{-1} s^{-1})
NADPH	experimental	5.25 ± 0.19	9.8 ± 1.3	(5.4 ± 0.9) × 10^5
	simulated[b]	6.6	14	4.7 × 10^5
DXP	experimental	5.25 ± 0.19	115 ± 7	(4.6 ± 0.3) × 10^4
	simulated[b]	6.1	98	6.2 × 10^4
$NADP^+$	experimental	0.95 ± 0.06	420 ± 40	(2.3 ± 0.2) × 10^3
	simulated[b]	1.04	438	2.4 × 10^3
MEP	experimental	0.95 ± 0.06	84 ± 9	(1.13 ± 0.14) × 10^4
	simulated[b]	1.11	196	5.7 × 10^3

[a]At pH 7.5 and 25 °C in the presence of 10 mM Mg^{2+}. Uncertainties are curve-fitting errors from nonlinear regression to eq 1. [b]Simulated from globally fitted model in Scheme 2.

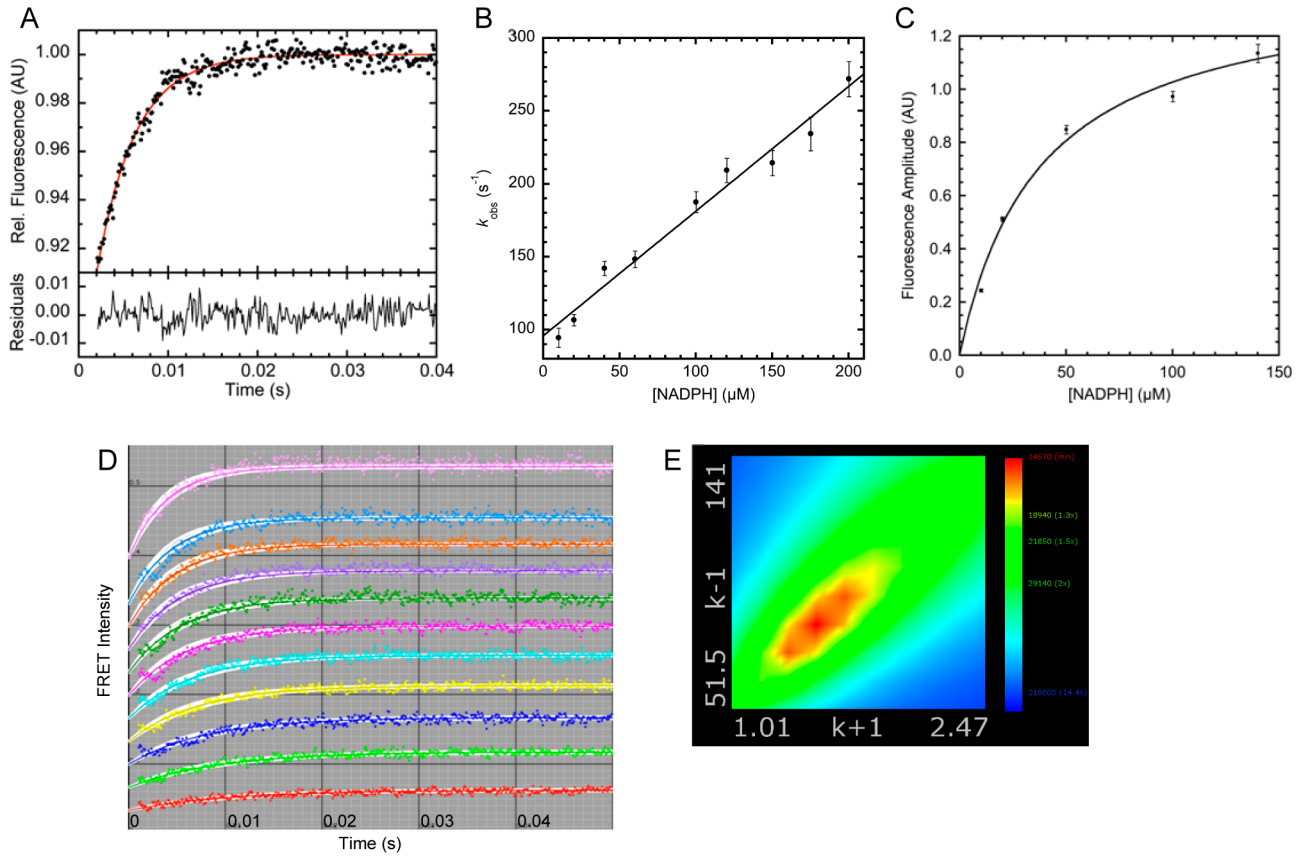

Figure 1. Binding kinetics of NADPH to *Mt*DXR. (A) Representative transient for 100 μM NADPH mixed with 1 μM *Mt*DXR, monitored by FRET (excitation at 290 nm, emission >395 nm). A single-exponential equation (eq 2) was best fitted to the data, and residuals are provided below the curve. A double-exponential equation did not improve the fit. (B) Observed rate constants (k_{obs}) were plotted versus NADPH concentration, and the rate constants were obtained by fitting a linear equation (eq 3). (C) Equilibrium dissociation constant for NADPH was obtained from a hyperbolic fit to a plot of FRET amplitude versus NADPH concentration. (D) Global fit of a one-step binding model to the binding transients (from bottom to top: 10, 20, 30, 40, 50, 60, 70, 80, 90, 100, and 120 μM NADPH) using KinTek Global Kinetic Explorer. White curves represent fits at the upper and lower boundaries of the parameter estimates obtained from the FitSpace confidence contour analysis[19] shown in (E).

saturating concentration of the cosubstrate (Table 1). Whereas the turnover number for the forward direction, $k_{cat,f}$ = 5.25 s^{-1}, is more than twice the value previously reported, that for the reverse direction, $k_{cat,r}$ = 0.95 s^{-1}, is comparable.[7] The K_m values of the substrates were found to be about twice as large as those previously reported.

Transient Kinetics of Binary Complex Formation. Substrate binding kinetics was monitored by the quenching of the protein's intrinsic tryptophan fluorescence or by fluorescence resonance energy transfer (FRET) in the case of NADPH, upon binary complex formation.[b] The FRET increase was best fitted with a single-exponential decay at all NADPH concentrations examined (Figure 1A). The observed rate constants varied linearly with NADPH concentration (Figure 1B and Table 2), suggestive of a one-step binding process. By plotting the amplitude of the FRET increase versus NADPH concentration (Figure 1C), a K_d of 34 ± 7 μM was obtained, which is approximately half of the ratio of off and on rate constants (64 μM). Simulation using KinTek Global Kinetic Explorer (Figure 1D) gave rate constants in excellent agreement with those of the analytical treatment and a K_{-1} of 54 μM, closer to the observed K_d from FRET amplitude. Table

dx.doi.org/10.1021/bi300513r | *Biochemistry* 2012, 51, 5307−5319

Table 2. Substrate Binding Rate Constants[a]

enzyme species	ligand	fitting	k_1 (μM^{-1} s^{-1})	k_{-1} (s^{-1})	k_2 (s^{-1})	k_{-2} (s^{-1})
E	NADPH	analytical	1.47 ± 0.04	93.8 ± 2.0		
		global, best fit	1.49 ± 0.04	80.4 ± 0.7		
		FitSpace range	1.34−1.78	71.4−101		
		scheme assignt	k_1	k_{-1}		
E	MEP	analytical	K_{-1} = 1480 μM[b]		223 ± 8	16.4 ± 0.5
		global, best fit	1000[c]	1080000 ± 30000	181 ± 4	17.3 ± 0.3
		FitSpace range		815000−1490000	139−246	14.6−20
		scheme assignt	k_{-8}	k_8	k_{-7}	k_7
E·NADPH	MEP	analytical	K_{-1} = 147 ± 2 μM[b]		31.6 ± 0.3	8.47 ± 0.06
		global, best fit	1000[c]	180000 ± 2000	19.8 ± 0.3	12.03 ± 0.10
		FitSpace range		138000−288000	15.8−30.9	9.62−15.5
		scheme assignt	k_{-14}	k_{14}	k_{-13}	k_{13}
E·MEP	NADPH	analytical	2.44 ± 0.14	72 ± 11	25 ± 5	20 ± 5
		global, best fit	1.92 ± 0.02	188 ± 2	30.6 ± 0.3	21.1 ± 0.2
		FitSpace range	1.53−2.68	150−264[d]	24.5−40.1	16.9−27.7
		scheme assignt	k_{11}	k_{-11}	k_{12}	k_{-12}

[a]The subscripts 1, −1, 2, and −2 for the rate constants indicate the steps involved in the one- or two-step binding process. The corresponding steps in the multistep mechanisms in Figure 3 and Scheme 2 are also indicated. Uncertainties reported for analytical and globally fitted values are standard errors from nonlinear regression. A more meaningful error estimation is provided by the FitSpace range.[19] [b]This step was too fast to observe directly. The apparent equilibrium constant was determined from the hyperbolic dependence of k_{obs} versus [MEP]. [c]Value was fixed at the diffusion limit during FitSpace analysis. [d]Calculated from $k_1 \times K_{-1}$.

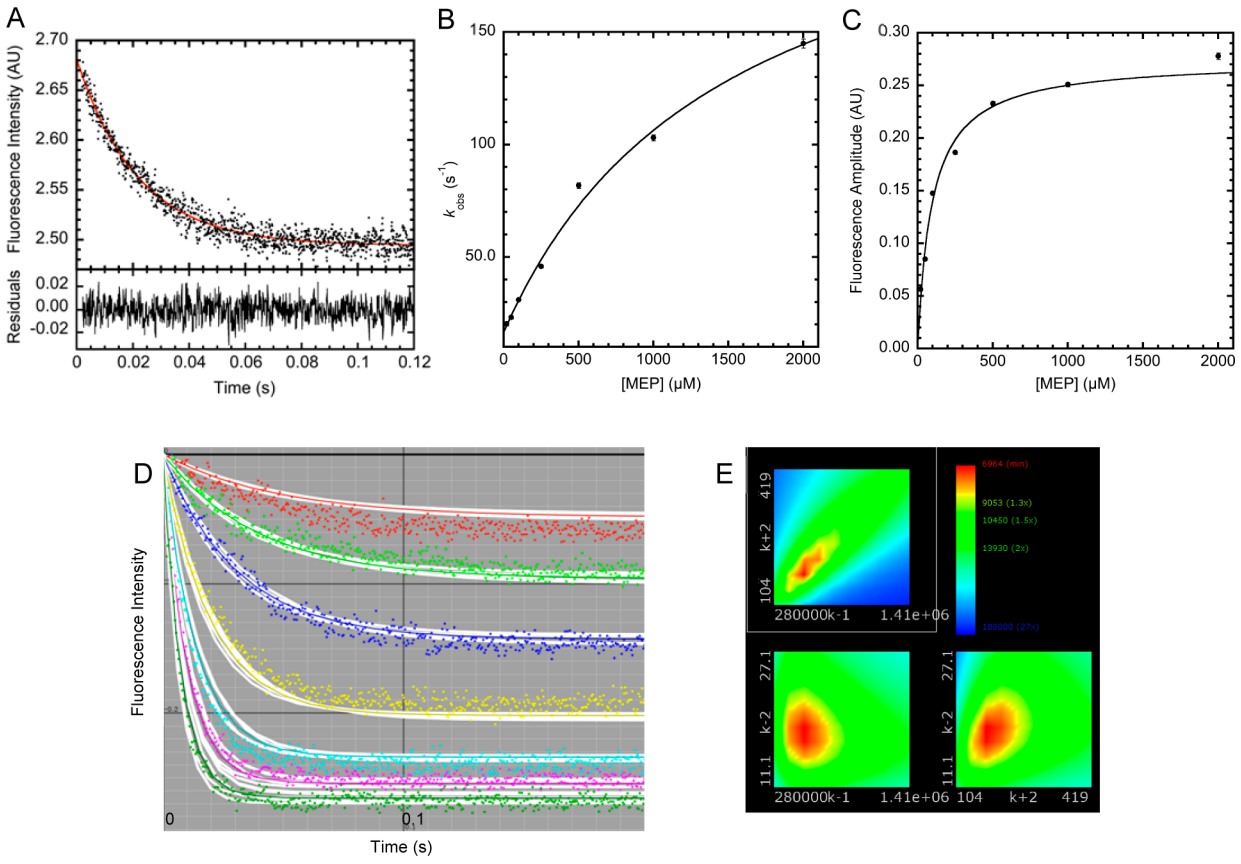

Figure 2. Binding kinetics of MEP to *Mt*DXR. (A) Representative transient for 250 μM MEP mixed with 1 μM *Mt*DXR, monitored by fluorescence (excitation at 290 nm, emission >320 nm). A single-exponential equation (eq 2) was best fitted to the data, and residuals are provided below the curve. A double-exponential equation did not improve the fit. (B) Observed rate constants (k_{obs}) were plotted versus MEP concentration, and the rate constants were obtained by fitting a hyperbolic equation (eq 4). (C) Equilibrium dissociation constant for MEP was obtained from a hyperbolic fit to a plot of fluorescence quench amplitude versus MEP concentration. (D) Global fit of a two-step binding model to the binding transients (from top to bottom: 20, 50, 100, 250, 500, 1000, and 2000 μM MEP) using KinTek Global Kinetic Explorer. White curves represent fits at the upper and lower boundaries of the parameter estimates obtained from the FitSpace confidence contour analysis[19] shown in (E).

dx.doi.org/10.1021/bi300513r | *Biochemistry* 2012, 51, 5307−5319

2 provides a comparison of the binding rate constants obtained by analytical and global fitting approaches.

Protein fluorescence quenching upon binding of MEP was also characterized by a single-exponential decay function (Figure 2A). The plot of the derived k_{obs} versus MEP concentration was best fitted with a hyperbolic equation, consistent with a two-step binding model (Figure 2B). Because no additional transient phases could be detected over the full range of MEP concentrations, rapid equilibrium binding followed by a slow conformational change was assumed.[20] A dissociation constant of 1.48 ± 0.10 mM (K_8 in Scheme 2) was

Scheme 1. Burst Kinetics Model for Pre-Steady-State Experiments with *Mt*DXR

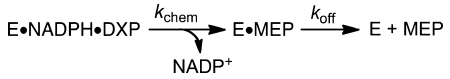

Scheme 2. Kinetic Mechanism for the Reaction Catalyzed by *Mt*DXR[a]

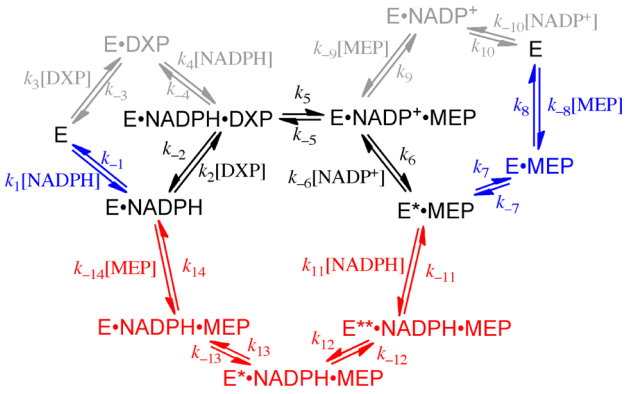

[a]Segments exclusive to the preferred and less favored pathways involving free enzyme (E) are blue and gray, respectively; segments exclusive to the pathway involving the nonproductive E·NADPH·MEP complexes are red; segments common to multiple pathways are black. Values for rate constants are provided in Tables 2 and 4.

estimated for the initial E·MEP complex, and forward and reverse rate constants of 223 ± 8 s^{-1} (k_{-7}) and 16.4 ± 0.5 s^{-1} (k_7), respectively, were obtained for the subsequent conformational change. The net dissociation constant, calculated as 101 ± 9 μM (eq 7), is in good agreement with the value of 95.9 ± 1.5 μM obtained from a plot of quench amplitude versus MEP concentration (Figure 2C). Global fitting of a two-step mechanism to the data provided excellent agreement (Figure 2D and Table 2), and the FitSpace confidence contours (Figure 2E) indicate that the system is well constrained. To achieve convergence in the model, it was necessary to fix k_{-8}, the rate constant for the initial, fast phase, at the diffusion limit (1000 μM^{-1} s^{-1}); thus, the related value of 1.08 × 10^6 s^{-1} for k_8 is also an upper limit, and it is the ratio of these constants (K_8 = 1080 μM) that is well-defined.

Attempts to measure rapid kinetics for binding of DXP and $NADP^+$ to *Mt*DXR were unsuccessful, as no significant fluorescence change was detectable in either case. The lack of observable transients could indicate that either binding occurs within the dead time of the stopped-flow instrument (1 ms) or no binding occurs for the ligand to the free enzyme. When titration was performed at equilibrium in a fluorometer, both substrates demonstrated quenching of the intrinsic tryptophan fluorescence, but positive curvature was observed in the Stern–Volmer plots (Figure S1 of the Supporting Information). In the case of $NADP^+$, the curvature could be attributed to inner filter effects, and by limiting the data to concentrations less than 500 μM, a linear plot was obtained, yielding a K_d of 280 ± 50 μM (eq 10). In contrast, DXP does not exhibit inner filter effects up to 10 mM. In this case, the positive deviations in the Stern–Volmer plot may be explained by simultaneous dynamic (i.e., diffusive collision) and static (i.e., binding) quenching mechanisms.[c] This behavior has been observed in systems with multiple fluorophores (*Mt*DXR has six tryptophan residues), and deconvolution can be challenging.[23] In another attempt to address binding of DXP to unliganded *Mt*DXR, equilibrium binding was performed with radioactively labeled DXP. No significant binding could be detected up to 250 μM DXP; nonspecific binding to the ultrafiltration membrane prevented accurate measurement at higher concentrations. In lieu of a directly determined value, a K_d of 630 ± 90 μM was estimated from eq 11, which is derived from the Haldane relationship for random mechanisms.[1]

$$K_d^{DXP} K_m^{NADPH} = K_d^{NADPH} K_m^{DXP} \quad (11)$$

Although the formation of a *Mt*DXR·DXP complex was inconclusive from the binding experiments, its existence is implied by the finding of Argyrou and Blanchard that the deuterium *V*/*K* KIE for [4-^{2}H]NADPH reaches a nonunitary value at an infinite concentration of DXP.[7] If DXP were to bind solely to the *Mt*DXR·NADPH complex, then the KIE would be expected to reach unity at infinite DXP. Additional evidence for binding of DXP to the free enzyme is the competitive inhibition by MEP (Table 3),[7] which indicates that the two substrates

Table 3. Product Inhibition Patterns[a]

product inhibitor	varied substrate	fixed substrate (concn)	pattern	reference
MEP	DXP	NADPH (10 μM)	competitive	ref 7
MEP	NADPH	DXP (50 μM)	noncompetitive	ref 7
$NADP^+$	DXP	NADPH (10 μM)	noncompetitive	ref 7 and this work
		NADPH (200 μM)	noncompetitive	this work
$NADP^+$	NADPH	DXP (50 μM)	noncompetitive	ref 7 and this work
		DXP (1 mM)	competitive	this work

[a]At pH 7.5 and 25 °C in the presence of 10 mM Mg^{2+}.

bind to the same enzyme form (i.e., free enzyme) or to forms that are in rapid equilibrium. This pattern excludes the existence of other enzyme forms to which only MEP binds unless they are joined by a rapid-equilibrium segment. Thus, this implies that either MEP does not bind to the *Mt*DXR·$NADP^+$ product complex—assuming it exists—or that $NADP^+$ dissociates rapidly, as is suggested by the lack of observable transient fluorescence changes.

Transient Kinetics of Nonproductive *Mt*DXR·NADPH··MEP Complex Formation. As has been observed in many dehydrogenases, it is possible that the reduced product (i.e., MEP) can mimic the oxidized substrate (i.e., DXP) by binding to NADPH-bound form of the protein (i.e., *Mt*DXR·NADPH) to generate a nonproductive complex (i.e., *Mt*DXR·NADPH··MEP). By binding to both free enzyme and *Mt*DXR·NADPH, MEP would be expected to yield an overall noncompetitive

dx.doi.org/10.1021/bi300513r | *Biochemistry* 2012, 51, 5307–5319

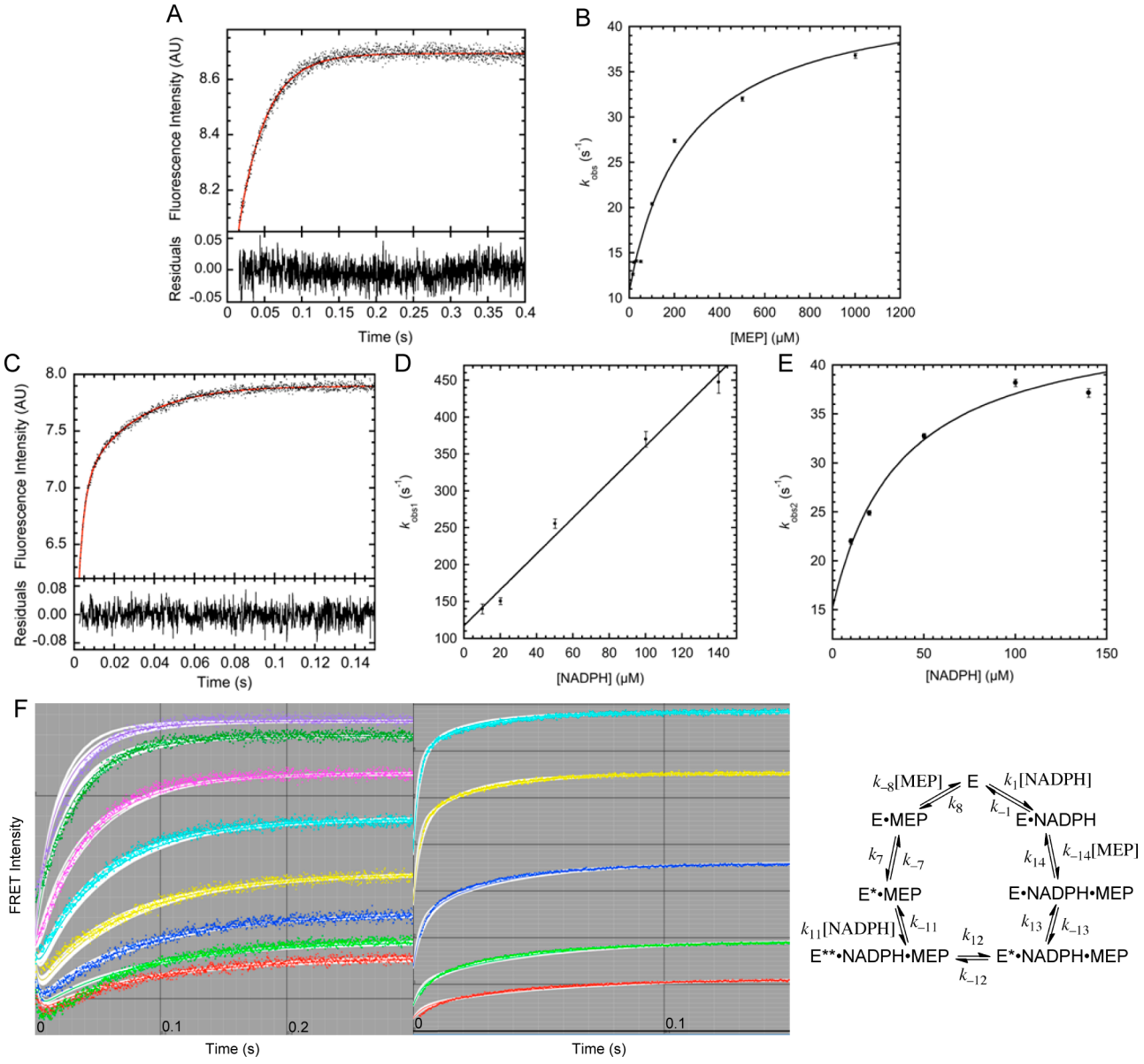

Figure 3. Kinetics of *Mt*DXR·NADPH·MEP formation. (A) Representative transient for 200 μM MEP mixed with 4 μM *Mt*DXR premixed with 200 μM NADPH, monitored by FRET (excitation at 290 nm, emission >395 nm). A single-exponential equation (eq 2) was best fitted to the data, and residuals are provided below the curve. A lag period of 15 ms, which can be seen in panel F, has been excluded for the purposes of analytical fitting. (B) Observed rate constants (k_{obs}) were plotted versus MEP concentration, and the rate constants were obtained by fitting a hyperbolic equation (eq 4). (C) Representative transient for 100 μM NADPH mixed with 2 μM *Mt*DXR premixed with 1000 μM MEP, monitored by FRET. A double-exponential equation was best fitted to the data, and residuals are provided below the curve. (D, E) Observed rate constants (k_{obs1} and k_{obs2}) were plotted versus NADPH concentration, and linear (D; eq 5) and hyperbolic (E; eq 6) functions were best fitted to the data. (F) Global fit of the mechanism (right) to the transients for binding varying MEP (left; from bottom to top: 15, 20, 30, 50, 100, 200, 500, and 1000 μM) or NADPH (middle; from bottom to top: 10, 20, 50, 100, and 140 μM) to the respective preformed binary complexes. k_1, k_{-1}, k_7, k_{-7}, k_8, and k_{-8} were fixed during global fitting at their best-fit values (Table 2). White curves represent fits at the upper and lower boundaries of the parameter estimates obtained from the FitSpace confidence contour analysis (Figure S7).

inhibition pattern against NADPH and a competitive pattern against DXP, and this is what has been observed (Table 3). When the *Mt*DXR·NADPH binary complex was mixed with MEP, a single-exponential increase in the FRET signal was observed (Figure 3A). A FRET enhancement upon addition of MEP under equilibrium conditions has also been noted for *E. coli* DXR.[24] A hyperbolic MEP concentration dependence of k_{obs} was obtained (Figure 3B), indicating that MEP binds in a multistep process, as it does to the free enzyme, where the first step is rapid-equilibrium formation of a loose complex prior to a slower conformational change to a tighter complex. Nonlinear regression (eq 4) provided estimated values of K_{14} = 147 ± 2 μM, k_{-13} = 31.6 ± 0.3 s^{-1}, and k_{13} = 8.47 ± 0.06 s^{-1}, indicating that MEP binds more tightly ($K_{d,net}$ = 31.1 ± 0.3 μM) and dissociates more slowly than in the absence of NADPH. As will be described in pre-steady-state experiments below, these characteristics impact catalytic turnover.

A double-exponential FRET signal was observed upon complexation of NADPH with *Mt*DXR·MEP (Figure 3C). The fast and slow observed rate constants displayed linear and

dx.doi.org/10.1021/bi300513r | *Biochemistry* 2012, 51, 5307−5319

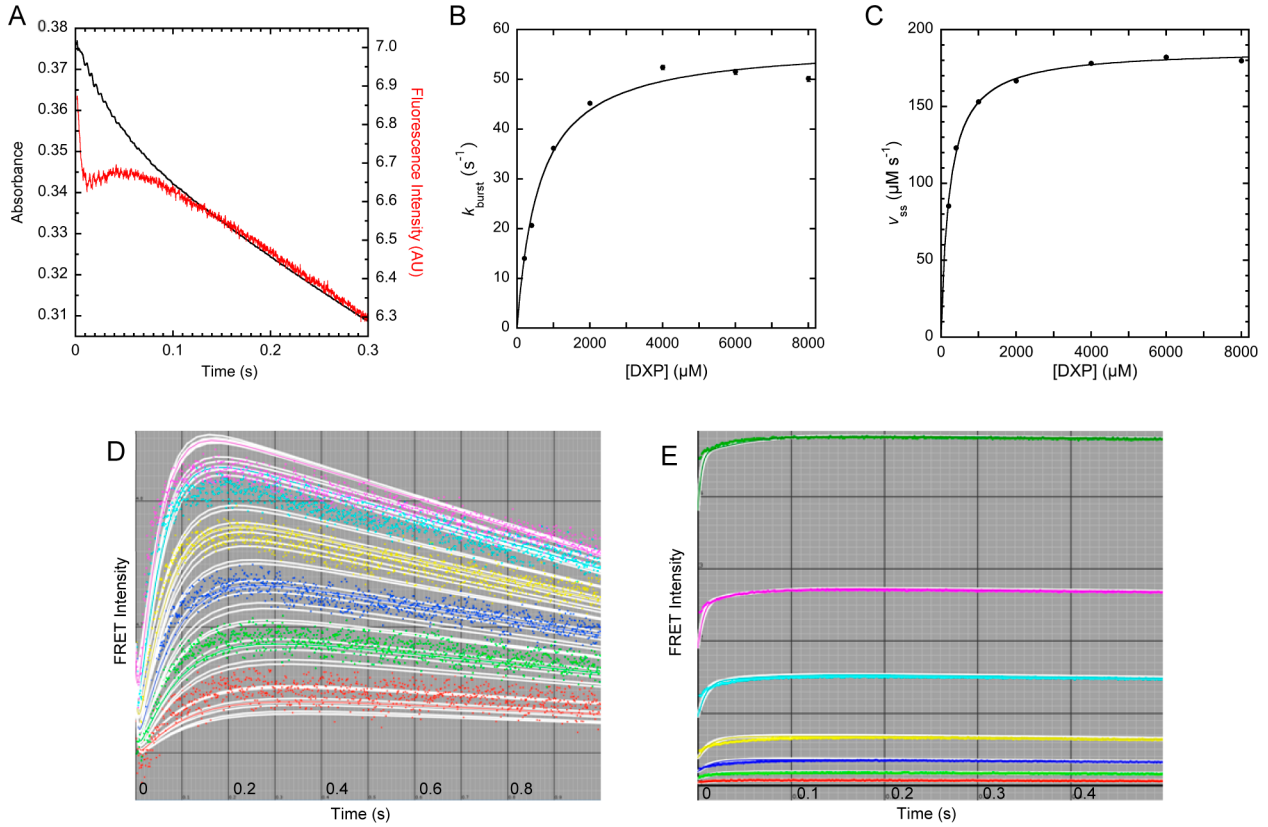

Figure 4. Pre-steady-state kinetics. (A) Representative absorbance (black) and fluorescence (red) transients recorded simultaneously upon mixing 1 mM DXP with 30 μM *Mt*DXR premixed with 320 μM NADPH (excitation at 340 nm, emission >395 nm). A burst equation (eq 8) was fitted to the absorbance data. (B, C) The burst rate constant, k_{burst}, (B) and steady-state rate, v_{ss}, (C) were plotted versus DXP concentration, and a hyperbolic equation (eq 4) was fitted to each. (D) Pre-steady-state fluorescence transients for mixing of DXP (bottom to top: 20, 50, 100, 200, 500, and 1000 μM) with 1 μM *Mt*DXR premixed with 200 μM NADPH (excitation at 290 nm, emission >395 nm). (E) Pre-steady-state fluorescence transients for mixing of NADPH (bottom to top: 2, 5, 10, 20, 50, 100, and 200 μM) with 1 μM *Mt*DXR premixed with 1 mM DXP. White curves in (D) and (E) represent fits at the upper and lower boundaries of the parameter estimates obtained from the FitSpace confidence contour analysis (Figure S8B of the Supporting Information) from global fitting to all turnover experiments.

hyperbolic concentration dependences, respectively (Figure 3D,E), indicating that NADPH binds in a multistep process. Linear regression (eq 5) for k_{obs1} provided a slope, k_{11}, of 2.44 ± 0.14 μM^{-1} s^{-1}, and intercept, $k_{-11} + k_{12} + k_{-12}$, of 117 ± 11 s^{-1}. Nonlinear regression (eq 6) for k_{obs2} yielded a maximal value, $k_{12} + k_{-12}$, of 45.3 ± 1.0 s^{-1}, which allowed for determination of $k_{-11} = 72 \pm 11$ s^{-1}. When [NADPH] = 0, eq 6 reduces to eq 12:

$$k_{obs2} = \frac{k_{-11}k_{-12}}{k_{-11} + k_{12} + k_{-12}} \quad (12)$$

Combining the *y*-intercept, 15.2 ± 0.9 s^{-1}, with the *y*-intercept from the linear plot of k_{obs1} allows one to solve $k_{-12} = 25 \pm 5$ s^{-1} and $k_{12} = 20 \pm 5$ s^{-1}. Thus, the $K_{d,net}$ for NADPH binding to the product complex is 17 μM (eq 7), about half that in the absence of MEP.

Global fitting of the two sets of experiments required a mechanism incorporating three conformations of the ternary complex (Figure 3F). In this model, E·NADPH and the first ternary complex (E·NADPH·MEP), which forms during the rapid equilibrium step of MEP binding, exhibit the same molar fluorescence, while the second (E*·NADPH·MEP) and third (E**·NADPH·MEP) complexes share a larger molar fluorescence. In the scheme in Figure 3F, the rate constants governing binary complex formation were fixed at their best-fit values, and all other constants were allowed to vary. The system failed to converge but FitSpace analysis indicated a strong correlation between k_{11} and k_{-11}, so their ratio (K_{-11} = 98.3 μM) was fixed. Likewise, k_{14} and k_{-14} were well correlated and large (i.e., rapid equilibrium), so k_{-14} was fixed at the diffusion limit, 1000 μM s^{-1}. Convergence (Figure S7 of the Supporting Information) was then achieved, yielding the rate constants provided in Table 2.

Pre-Steady-State Kinetics and Formation of *Mt*DXR·NADPH·MEP Complex during Turnover. Kinetic isotope effect experiments by Argyrou and Blanchard using deuterated NADPH revealed a primary *V*/*K* KIE of 2.2 with DXP as the variable substrate.[7] This result indicates that the reduction step is at least partially rate limiting on the parameter k_{cat}/K_m, which reflects steps from binding up to and including the first irreversible step, likely release of the first product. The KIE on V_{max} of 1.3, on the other hand, is significantly lower. The difference between *V*/*K* and *V* KIEs arises in the rate constants that make up their respective forward commitments to catalysis, C_f and C_{vf}.[1] Although both parameters reflect all steps following formation of the ternary complex up to the isotope-sensitive step (i.e., reduction), C_f additionally involves steps governing substrate binding, while C_{vf} additionally involves steps following reduction, including product release and/or conformational changes. Since larger commitments lead

dx.doi.org/10.1021/bi300513r | *Biochemistry* 2012, 51, 5307−5319

Table 4. Rate Constants from Global Fitting of Scheme 2[a]

rate constant	best-fit value	FitSpace range	rate constant	best-fit value	FitSpace range
k_2 (μM^{-1} s^{-1})		1000[b]	k_{-5} (s^{-1})	1.322 ± 0.003	1.18−1.51
k_{-2} (s^{-1})	338000 ± 1500	270000−434000	k_6 (s^{-1})	466000 ± 2000	372000−599000
k_3 (μM^{-1} s^{-1})		1000[b]	k_{-6} (μM^{-1} s^{-1})		1000[b]
k_{-3} (s^{-1})		543000[c]	k_9 (s^{-1})		~0[e]
k_4 (μM^{-1} s^{-1})	2.08 ± 0.03	0.85−5.07	k_{-9} (μM^{-1} s^{-1})		~0[e]
k_{-4} (s^{-1})	69.8 ± 0.3	55.8−91.7[d]	k_{10} (s^{-1})	358600 ± 1100	303000−413000
k_5 (s^{-1})	28.18 ± 0.13	22.5−37.0[d]	k_{-10} (μM^{-1} s^{-1})		1000[b]

[a]Rate constants associated with binding of NADPH and MEP are in Table 2. Uncertainties reported for best-fit values are standard errors from nonlinear regression. A more meaningful error estimation is provided by the FitSpace range.[19] [b]Rate constant was fixed at diffusion limit since fitting indicated the rate constant was >100 μM^{-1} s^{-1}. [c]Optimized to satisfy thermodynamics: $K_3K_4 = K_1K_2$. [d]Calculated as best-fit value × (k_{-2} FitSpace range)/(k_{-2} best-fit value). [e]Value is negligibly small, $<10^{-4}$.

to lower observed KIEs, C_{vf} must be larger than C_f, and therefore, we hypothesized that a slow step follows reduction.

Transient kinetics measurements were performed under multiple-turnover conditions to determine if a slow step follows hydride transfer and therefore yields a kinetic burst. Indeed, when monitoring absorbance in the DXP isomerization−reduction direction, a significant burst was observed that was approximately stoichiometric with enzyme concentration (Figure 4A, black curve). The DXP concentration was varied, and the series of transients were fitted with eq 8 to provide a series of k_{burst}, v_{ss}, and amplitude values. While the amplitudes appeared to be largely independent of DXP, reaching an average value of 19.1 ± 1.3 μM, k_{burst} and v_{ss} varied hyperbolically (Figure 4B,C). Maximal k_{burst} and v_{ss} values were 57.2 ± 1.8 s^{-1} and 187.1 ± 1.5 μM s^{-1}, respectively, and an apparent dissociation constant of 610 ± 110 μM for DXP from the ternary complex was estimated from the k_{burst} plot. Burst kinetics are often interpreted in terms of a two-step irreversible mechanism (Scheme 1), which involves only (1) chemistry and release of the first product and (2) release of the second product.[20] In this model, the substrate is assumed to bind in rapid equilibrium, which is suggested by the absence of any additional exponential phases under all concentrations used.[1] Based on our binding studies, MEP is released substantially more slowly (17.3 s^{-1} from *Mt*DXR·MEP and 12.0 s^{-1} from *Mt*DXR·NADPH·MEP) than $NADP^+$ and is therefore the second product to dissociate in this simplified model. In Scheme 1, k_{cat} is given by the net rate constants for chemistry, k_{chem}, and MEP release, k_{off}[25]

$$k_{cat} = \frac{k_{chem}k_{off}}{k_{chem} + k_{off}} \quad (13)$$

The maximum k_{burst} (eq 9) is equal to $k_{chem} + k_{off}$, and the burst amplitude, $[NADP^+]_{burst}$, is given by

$$[NADP^+]_{burst} = [E]_{act}\left(\frac{k_{chem}}{k_{chem} + k_{off}}\right)^2 \quad (14)$$

where $[E]_{act}$ is the total active enzyme concentration.[21,22] Together with $v_{ss,max} = k_{cat}[E]_{act}$, the above equations can be solved to yield k_{cat} = 7.1 ± 0.5 s^{-1}, $[E]_{act}$ = 26.4 ± 1.8 μM, k_{chem} = 48.8 ± 1.9 s^{-1}, and k_{off} = 8.4 ± 0.5 s^{-1}. The k_{cat} value is in reasonable agreement with that obtained in steady-state experiments. The value of k_{off} is about half that for release of MEP from the binary complex and is similar to its release from the nonproductive ternary complex with NADPH. Finally, since 30 μM *Mt*DXR was used in these experiments, the enzyme can be estimated to be 88 ± 11% catalytically active, assuming negligible reverse reaction contributes to the burst (see below).

The burst analysis indicates that catalysis is limited by product release. This result contrasts the findings of Fox and Poulter, who reported the absence of a burst in multiple-turnover experiments with *E. coli* DXR.[26] The similarity in magnitude of k_{off} to the apparent dissociation constant for MEP from the *Mt*DXR·NADPH·MEP complex (k_{13}) led us to speculate that this species may be generated during turnover. Intriguingly, concurrent with the burst phase that was monitored by absorbance, NADPH fluorescence displayed an initial fast decrease followed by a recovery before ultimately leading to a linear decrease (Figure 4A, red curve). The rapid and linear decreases in NADPH fluorescence can be attributed to oxidation during the first turnover and steady state, respectively, while the increase is suggestive of the formation of *Mt*DXR·NADPH·MEP. To verify that this increase was not due to formation of the reactive *Mt*DXR·NADPH·DXP complex, single-turnover reactions were performed with substoichiometric NADPH (Figure S2 of the Supporting Information). Under these conditions, the fluorescence recovery was no longer detectable, indicating that most of the limiting NADPH had oxidized before it could bind to the product *Mt*DXR·MEP complex. When the magnitude of the burst phase was decreased by lowering the enzyme concentration in multiple-turnover conditions to 1 μM, the fluorescence increase was emphasized (Figure 4D), and a strong resemblance to the transients in Figure 3F is apparent. Reversal of the order of substrate mixing with *Mt*DXR also resulted in a burst decrease in absorbance (data not shown) and increase in fluorescence (Figure 4E). It should be noted that the increase in fluorescence is detectable with either 290 or 340 nm excitation, and therefore the effect is attributable to changes in NADPH emission.

Multiple-turnover experiments in the MEP oxidation−isomerization direction with either order of substrate premixed with enzyme did not exhibit burst kinetics. The lack of a detectable burst can be explained by (1) MEP oxidation or a step preceding it is rate limiting, (2) the internal equilibrium (K_{int}) strongly favors the reduction direction, or (3) both.[20] A large K_{int} would predict a full burst amplitude in the forward direction, which was approximately demonstrated by the 88% active protein calculated above.

Global Fitting and Steady-State Kinetic Mechanism of *Mt*DXR. All multiple-turnover experiments were fitted simultaneously with KinTek Global Kinetic Explorer to the mechanism in Scheme 2 (Table 4). In this mechanism, a random order of substrate and product binding was included,

dx.doi.org/10.1021/bi300513r | *Biochemistry* 2012, 51, 5307−5319

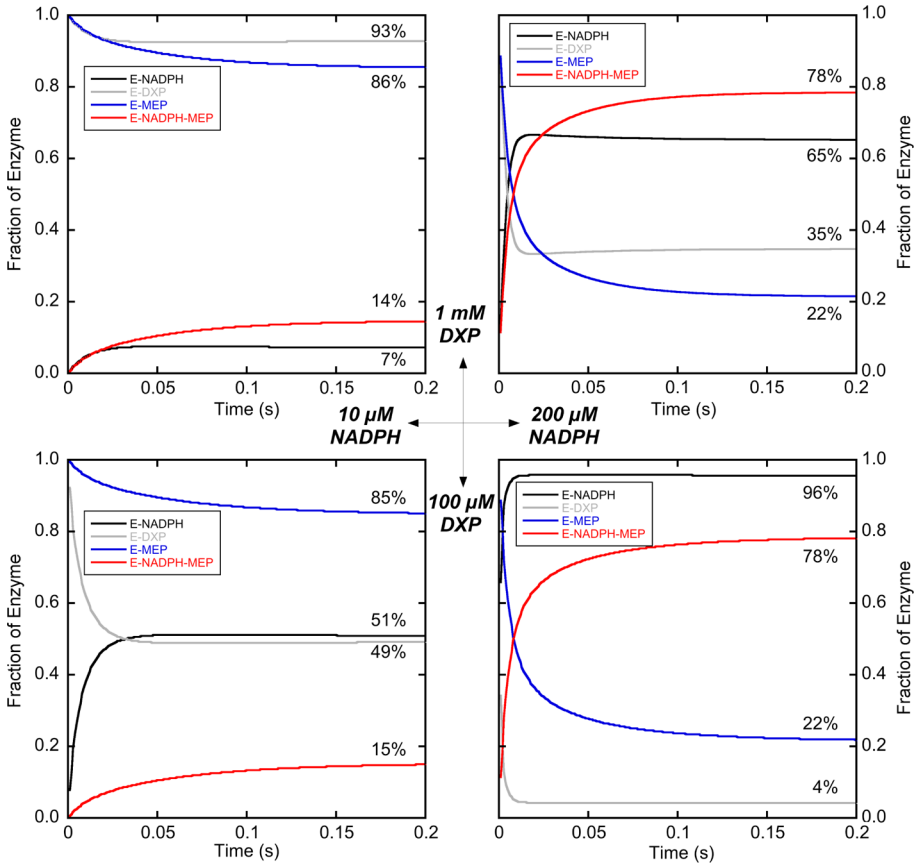

Figure 5. Partitioning of *Mt*DXR into parallel substrate-binding and product-release pathways. Data were simulated with KinTek Global Kinetic Explorer under saturating and subsaturating concentrations of DXP and NADPH in the presence of 1 μM *Mt*DXR. Counterclockwise from top-right quadrant: 200 μM NADPH, 1 mM DXP; 10 μM NADPH, 1 mM DXP; 10 μM NADPH, 100 μM DXP; 200 μM NADPH, 100 μM DXP. Curves reflect the relative distribution of reactant complexes (E-NADPH, black; E-DXP, gray) and product complexes (E-MEP, blue; E-NADPH-MEP, red).

along with the alternative product release pathway via *Mt*DXR·NADPH·MEP. It was necessary to constrain several parameters to achieve a well-defined global fit. First, during the fitting process, it became clear that DXP and $NADP^+$ bind in rapid equilibrium steps, and so, their respective on-rate constants were fixed at the diffusion limit (1000 μM^{-1} s^{-1}). Second, although the K_d for DXP could not be measured directly, we initially set k_{-3} to match the K_d of 630 μM estimated above from the Haldane relationship (eq 11). After nonlinear regression, however, it was found that the overall equilibrium constant for the upper pathway (K_3K_4) exceeded that for the lower pathway (K_1K_2). k_{-3} was then iteratively varied, and all other rate constants were reoptimized until the ratio K_3K_4/K_1K_2 reached unity, which occurred at k_{-3} = 543 000 s^{-1} (Figure S8A in Supporting Information). Third, after fixing k_{-3} at this value, k_{-2}, k_{-4}, and k_5 were found to be strongly correlated, so their ratios were held constant. Finally, the ratio k_9/k_{-9} governing release of MEP from its ternary product complex was restricted to satisfy the thermodynamic box ($K_6K_7K_8 = K_9K_{10}$).

Global nonlinear regression indicated that k_9 and k_{-9} are negligibly small, suggesting that MEP is not released from the product ternary complex and therefore that $NADP^+$ dissociation strictly precedes MEP. This order of product release differs from the one purported for *E. coli* DXR[6,27] and which is commonplace for most dehydrogenases and reductases, in which the coenzyme is the first to bind and last to dissociate. Since the *E. coli* enzyme does not exhibit burst kinetics, it is apparent that *Mt*DXR is exceptional in its slow release of MEP. It is noteworthy that the enzymes from these organisms exhibit distinct thermodynamic properties with respect to inhibitor binding,[28] and this may relate to the differences in their kinetic mechanisms.

As a check for the validity of this model, steady-state kinetics were simulated with the globally derived rate constants to mimic the reactions measured spectrophotometrically (Table 1). This approach obviates the tedium of rate equation derivation for the complex mechanism in Scheme 2 while permitting qualitative assessment of kinetic parameters. The turnover numbers for both reaction directions and all Michaelis constants except for that of MEP were in good agreement with the experimental values. Further, it was found necessary to retain the segment for $NADP^+$ binding to the free enzyme; setting k_{10} and k_{-10} to 0 resulted in best-fit values of 0.82 s^{-1} for k_{-5}, which is lower than the k_{cat} for the reverse reaction direction, and the simulated K_m for MEP dropped to only 11 μM. The ratio of the best-fit values for k_{10} and k_{-10} (i.e., K_{10}) predicts a K_d for $NADP^+$ of 359 μM, which is in reasonable agreement with the value of 280 $\pm$ 50 μM obtained from fluorescence titration (see above).

The global analysis revealed that although NADPH is held more tightly than DXP in both binary and ternary reactant complexes, the rates of association and dissociation differ by several orders. Whereas DXP binds in rapid equilibrium, NADPH dissociates from the Michaelis complex at a rate (k_{-4} = 69.8 s^{-1}) comparable to chemistry (k_5 = 28.2 s^{-1}). As such,

dx.doi.org/10.1021/bi300513r | *Biochemistry* 2012, 51, 5307−5319

we have verified the assertion that NADPH is a sticky substrate while DXP is not, a conclusion that had been reached to explain the concentration dependence of kinetic isotope effects.[7]

The globally fitted forward and reverse rate constants for the chemical step, k_5 and k_{-5}, are 28.2 s^{-1} and 1.32 s^{-1}, respectively. These values indicate that the k_{chem} of 48.8 s^{-1} calculated in the analytical treatment above is slightly overestimated, perhaps indicating that the model in Scheme 1 is overly simplistic. Nevertheless, the K_{int} of 21.7 accounts for the observed burst magnitudes and confirms that the forward direction is favored on the enzyme. The overall equilibrium constant, K_{eq}', was calculated with eq 15 to be 56, which is in excellent agreement with values of 45,[8] 52,[7] and 69,[5] determined experimentally. This can additionally be compared with the value estimated from the Haldane relationship for Bi−Bi mechanisms (eq 16)

$$K'_{eq} = \frac{k_1k_2k_5k_6k_7k_8}{k_{-1}k_{-2}k_{-5}k_{-6}k_{-7}k_{-8}} \quad (15)$$

$$K'_{eq} = \frac{k_{cat,f}K_{iq}K_p}{k_{cat,r}K_{ia}K_b} \quad (16)$$

where K_{ia} and K_{iq} are the dissociation constants for the first substrate to bind (A) and last product to be released (Q), and K_b and K_p are the K_m for the second substrate (B) and first product (P), respectively.[29] The pathway with A = NADPH, B = DXP, P = $NADP^+$, and Q = MEP yields a value of 39, consistent with the previous estimates.

The free enzyme and MEP-bound binary complex represent two branch points in the mechanism under steady-state turnover. We investigated the relative flux through each of the parallel substrate-binding (i.e., via *Mt*DXR·NADPH or *Mt*DXR·DXP) and product-release (i.e., via *Mt*DXR or *Mt*DXR·NADPH·MEP) pathways by simulating steady-state data under saturating and subsaturating substrate concentrations (Figure 5). When both NADPH and DXP are near their K_m values, there is an equal probability for each substrate-binding pathway. As either substrate is increased to saturating levels, the corresponding pathway becomes favored; however, at saturating levels of both, there is a 2:1 preference for NADPH binding first. Whereas direct release of MEP from the binary complex is favored at low concentrations of NADPH, the nonproductive *Mt*DXR·NADPH·MEP accumulates as NADPH levels are brought to saturation. Binding of NADPH prior to release of the second product is a hallmark of dihydrofolate reductases (DHFR),[30−32] and intriguingly, *M. tuberculosis* DHFR was most recently shown to exhibit a similar parallel product release pathway.[33]

Product Inhibition by $NADP^+$. Having validated the feasibility of the kinetic mechanism in Scheme 2, it is appropriate to revisit the product inhibition patterns (Table 3). Whereas we have accounted for inhibition by MEP, the two noncompetitive patterns observed for $NADP^+$ have not been addressed. According to the global kinetic analysis, $NADP^+$ is capable of binding in rapid equilibrium to the MEP-bound and free forms of the enzyme, but since MEP does not bind appreciably to *Mt*DXR·$NADP^+$, this is effectively a dead-end complex. The fact that DXP is incapable of binding to *Mt*DXR·MEP and that this complex dissociates at steady-state rates explains the noncompetitive inhibition of $NADP^+$ versus DXP. The noncompetitive pattern against NADPH, however, is perplexing. According to Scheme 2, both cofactors are capable of binding to *Mt*DXR and *Mt*DXR·MEP, and as such, $NADP^+$ should display competitive inhibition. By increasing the concentration of the fixed cosubstrate to saturating levels, product inhibition patterns often change as a result of the introduction of an irreversible binding step. Thus, we investigated the inhibition by $NADP^+$ under saturating NADPH or DXP (Table 3). With NADPH at 200 μM, $NADP^+$ remained a noncompetitive inhibitor with respect to DXP; this is expected since the segment involving $NADP^+$ binding to *Mt*DXR·MEP is unaffected by the level of cosubstrate. With DXP at 1 mM, however, the pattern switched to competitive versus NADPH (Figure S9 of the Supporting Information). A plausible explanation is that the noncompetitive pattern observed at low DXP is the mixture of a competitive pattern and an uncompetitive pattern, which is removed when DXP is saturating. This implies the possibility that $NADP^+$ is capable of binding to the *Mt*DXR·NADPH complex—either to a different site or to the active site in the adjacent subunit of the dimer—to generate a hybrid *Mt*DXR·NADPH·$NADP^+$ complex, which has impaired catalytic activity. Under saturating DXP, the *Mt*DXR·NADPH complex is largely bypassed (Figure 5), and therefore, $NADP^+$ is forced to compete with NADPH for the MEP-bound enzyme. Although a similar hybrid complex has been proposed to form with betaine dehydrogenase,[34] in the absence of structural evidence, the existence of *Mt*DXR·NADPH·$NADP^+$ is speculative. Nevertheless, since the uncompetitive component of $NADP^+$ inhibition versus NADPH is so weak (K_{ii} = 2.5 mM),[7] such a hybrid complex is unlikely to form under normal reaction conditions.

CONCLUSIONS

We have evaluated the kinetic mechanism of *Mt*DXR by application of steady-state and pre-steady-state kinetics. Through analytical and global fitting approaches, we have demonstrated a steady-state mechanism with random binding of NADPH and DXP and ordered product release, with $NADP^+$ preceding MEP. Burst kinetics was observed under multiple-turnover conditions, indicating that MEP release is rate limiting on turnover. MEP dissociates from *Mt*DXR in parallel by direct release from the binary complex and by means of a NADPH-bound ternary intermediate, analogous to *M. tuberculosis* dihydrofolate reductase. Product inhibition patterns are reconciled in light of the details from this kinetic analysis. This is the first complete transient kinetic investigation into the mechanism of this important drug target.

ASSOCIATED CONTENT

Supporting Information

Stern−Volmer plots for $NADP^+$ and DXP, procedural details for [5-$^3H_1$]DXP synthesis and equilibrium binding by ultrafiltration and single-turnover reactions, a complete description of analytical and global data analysis for stopped-flow experiments, and double-reciprocal plot for product inhibition by $NADP^+$. This material is available free of charge via the Internet at http://pubs.acs.org.

AUTHOR INFORMATION

Corresponding Author

*E-mail: amurkin@buffalo.edu; Tel: (716) 645-4249; Fax: (716) 645-6963.

Present Address

[†]Department of Molecular, Microbial and Structural Biology, University of Connecticut Health Center, Farmington, CT 06030.

Funding

This work was supported by funding from the University at Buffalo, The State University of New York.

Notes

The authors declare no competing financial interest.

■ ACKNOWLEDGMENTS

We thank John S. Blanchard and John P. Richard for providing plasmids encoding DXP synthase and triose phosphate isomerase, respectively.

■ ABBREVIATIONS

DXP, 1-deoxy-D-xylulose 5-phosphate; MEP, 2-*C*-methyl-D-erithritol 4-phosphate; DXR, 1-deoxy-D-xylulose-5-phosphate reductoisomerase; *Mt*DXR, *Mycobacterium tuberculosis* DXR; KIE, kinetic isotope effect; CV, column volume; FRET, fluorescence resonance energy transfer.

■ ADDITIONAL NOTES

[a]Equilibrium binding of the second substrate is assumed, which is justified if $k_{-2} \gg k_5$ or $k_6 \gg k_{-5}$. This assumption is supported by computational simulations and is reflected in the lack of a second exponential component in the burst.[1]

[b]All experiments contained saturating Mg^{2+} (10 mM), and therefore it is assumed that it is bound in all complexes. Thus, the complexes referred to in this article as "free", "binary", and "ternary" are truly binary, ternary, and quaternary, respectively, when the metal is included.

[c]We have demonstrated that DXP is capable of nonspecific fluorescence quenching through dynamic processes by titrating it against isocitrate lyase, which possesses nine tryptophan residues (see Supporting Information, Figure S1). DXP is not expected to bind to this unrelated protein.

■ REFERENCES

(1) Cook, P. F., and Cleland, W. W. (2007) *Enzyme Kinetics and Mechanism*, Garland Science, New York.

(2) Rohdich, F., Kis, K., Bacher, A., and Eisenreich, W. (2001) The non-mevalonate pathway of isoprenoids: genes, enzymes and intermediates. *Curr. Opin. Chem. Biol. 5*, 535−540.

(3) Rodriguez-Concepcion, M., and Boronat, A. (2002) Elucidation of the methylerythritol phosphate pathway for isoprenoid biosynthesis in bacteria and plastids. A metabolic milestone achieved through genomics. *Plant Physiol. 130*, 1079−1089.

(4) Sprenger, G. A., Schorken, U., Wiegert, T., Grolle, S., de Graaf, A. A., Taylor, S. V., Begley, T. P., Bringer-Meyer, S., and Sahm, H. (1997) Identification of a thiamin-dependent synthase in Escherichia coli required for the formation of the 1-deoxy-D-xylulose 5-phosphate precursor to isoprenoids, thiamin, and pyridoxol. *Proc. Natl. Acad. Sci. U. S. A. 94*, 12857−12862.

(5) Hoeffler, J. F., Tritsch, D., Grosdemange-Billiard, C., and Rohmer, M. (2002) Isoprenoid biosynthesis via the methylerythritol phosphate pathway. Mechanistic investigations of the 1-deoxy-D-xylulose 5-phosphate reductoisomerase. *Eur. J. Biochem. 269*, 4446−4457.

(6) Munos, J. W., Pu, X. T., Mansoorabadi, S. O., Kim, H. J., and Liu, H. W. (2009) A Secondary Kinetic Isotope Effect Study of the 1-Deoxy-D-xylulose-5-phosphate Reductoisomerase-Catalyzed Reaction: Evidence for a Retroaldol-Aldol Rearrangement. *J. Am. Chem. Soc. 131*, 2048−2049.

(7) Argyrou, A., and Blanchard, J. S. (2004) Kinetic and chemical mechanism of Mycobacterium tuberculosis 1-deoxy-D-xylulose-5-phosphate isomeroreductase. *Biochemistry 43*, 4375−4384.

(8) Koppisch, A. T., Fox, D. T., Blagg, B. S., and Poulter, C. D. (2002) E. coli MEP synthase: steady-state kinetic analysis and substrate binding. *Biochemistry 41*, 236−243.

(9) Go, M. K., Amyes, T. L., and Richard, J. P. (2009) Hydron transfer catalyzed by triosephosphate isomerase. Products of the direct and phosphite-activated isomerization of [1-^{13}C]-glycolaldehyde in D_2O. *Biochemistry 48*, 5769−5778.

(10) Henriksson, L. M., Unge, T., Carlsson, J., Aqvist, J., Mowbray, S. L., and Jones, T. A. (2007) Structures of Mycobacterium tuberculosis 1-deoxy-D-xylulose-5-phosphate reductoisomerase provide new insights into catalysis. *J. Biol. Chem. 282*, 19905−19916.

(11) Cole, S. T., Brosch, R., Parkhill, J., Garnier, T., Churcher, C., Harris, D., Gordon, S. V., Eiglmeier, K., Gas, S., Barry, C. E., III, et al. (1998) Deciphering the biology of Mycobacterium tuberculosis from the complete genome sequence. *Nature 393*, 537−544.

(12) Gasteiger, E. H. C., Gattiker, A., Duvaud, S., Wilkins, M. R., Appel, R. D., and Bairoch, A. (2005) Protein identification and analysis tools on the ExPASy server, in *The Proteomics Protocols Handbook* (Walker, J. M., Ed.), pp 571−607, Humana Press, Totowa, NJ.

(13) Taylor, S. V., Vu, L. D., Begley, T. P., Schorken, U., Grolle, S., Sprenger, G. A., Bringer-Meyer, S., and Sahm, H. (1998) Chemical and enzymatic synthesis of 1-Deoxy-D-xylulose-5-phosphate. *J. Org. Chem. 63*, 2375−2377.

(14) Keinan, E., Hafeli, E. K., Seth, K. K., and Lamed, R. (1986) Thermostable enzymes in organic synthesis. 2. Asymmetric reduction of ketones with alcohol dehydrogenase from Thermoanaerobium brockii. *J. Am. Chem. Soc. 108*, 162−169.

(15) Dawson, R. M. C., Elliott, D. C., Elliott, W. H., and Jones, K. M. (1986) *Data for Biochemical Research*, 3rd ed., Clarendon Press, Oxford.

(16) O'Donoghue, A. C., Amyes, T. L., and Richard, J. P. (2005) Hydron transfer catalyzed by triosephosphate isomerase. Products of isomerization of (R)-glyceraldehyde 3-phosphate in D_2O. *Biochemistry 44*, 2610−2621.

(17) Johnson, K. A., Simpson, Z. B., and Blom, T. (2009) Global kinetic explorer: a new computer program for dynamic simulation and fitting of kinetic data. *Anal. Biochem. 387*, 20−29.

(18) Johnson, K. A. (2009) Fitting enzyme kinetic data with KinTek Global Kinetic Explorer. *Methods Enzymol. 467*, 601−626.

(19) Johnson, K. A., Simpson, Z. B., and Blom, T. (2009) FitSpace explorer: an algorithm to evaluate multidimensional parameter space in fitting kinetic data. *Anal. Biochem. 387*, 30−41.

(20) Johnson, K. A. (1992) Transient-State Kinetic Analysis of Enzyme Reaction Pathways, in *The Enzymes* (David, S. S., Ed.), pp 1−61, Academic Press, New York.

(21) Alexander, J. P., Ryan, T. J., Ballou, D. P., and Coward, J. K. (2008) gamma-Glutamyl hydrolase: Kinetic characterization of isopeptide hydrolysis using fluorogenic substrates. *Biochemistry 47*, 1228−1239.

(22) Bender, M. L., Kezdy, F. J., and Wedler, F. C. (1967) alpha-Chymotrypsin: Enzyme Concentration and Kinetics. *J. Chem. Educ. 44*, 84−88.

(23) Lakowicz, J. R. (2006) *Principles of Fluorescence Spectroscopy*, 3rd ed., Springer, New York.

(24) Munos, J. W. (2008) Ph.D. Thesis, The University of Texas at Austin.

(25) Cleland, W. W. (1975) Partition analysis and the concept of net rate constants as tools in enzyme kinetics. *Biochemistry 14*, 3220−3224.

(26) Fox, D. T., and Poulter, C. D. (2005) Mechanistic studies with 2-C-methyl-D-erythritol 4-phosphate synthase from Escherichia coli. *Biochemistry 44*, 8360−8368.

(27) Wong, A., Munos, J. W., Devasthali, V., Johnson, K. A., and Liu, H. W. (2004) Study of 1-deoxy-D-xylulose-5-phosphate reductoisomerase: synthesis and evaluation of fluorinated substrate analogues. *Org. Lett. 6*, 3625−3628.

(28) Cai, G., Deng, L., Fryszczyn, B. G., Brown, N. G., Liu, Z., Jiang, H., Palzkill, T., and Song, Y. (2012) Thermodynamic Investigation of Inhibitor Binding to 1-Deoxy-d-Xylulose-5-Phosphate Reductoisomerase. *ACS Med. Chem. Lett. 3*, 496−500.
(29) Cleland, W. W. (1982) An analysis of Haldane Relationships. *Methods Enzymol. 87*, 366−369.
(30) Fierke, C. A., Johnson, K. A., and Benkovic, S. J. (1987) Construction and evaluation of the kinetic scheme associated with dihydrofolate reductase from Escherichia coli. *Biochemistry 26*, 4085−4092.
(31) Thillet, J., Adams, J. A., and Benkovic, S. J. (1990) The kinetic mechanism of wild-type and mutant mouse dihydrofolate reductases. *Biochemistry 29*, 5195−5202.
(32) Andrews, J., Fierke, C. A., Birdsall, B., Ostler, G., Feeney, J., Roberts, G. C., and Benkovic, S. J. (1989) A kinetic study of wild-type and mutant dihydrofolate reductases from Lactobacillus casei. *Biochemistry 28*, 5743−5750.
(33) Czekster, C. M., Vandemeulebroucke, A., and Blanchard, J. S. (2011) Two parallel pathways in the kinetic sequence of the dihydrofolate reductase from Mycobacterium tuberculosis. *Biochemistry 50*, 7045−7056.
(34) Velasco-Garcia, R., Gonzalez-Segura, L., and Munoz-Clares, R. A. (2000) Steady-state kinetic mechanism of the NADP+- and NAD +-dependent reactions catalysed by betaine aldehyde dehydrogenase from Pseudomonas aeruginosa. *Biochem. J. 352* (Pt 3), 675−683.